



Geophysical Research Letters

RESEARCH LETTER

10.1029/2018GL081512

Key Points:

- An anticyclonic subthermocline eddy was documented by a mooring in the western equatorial Pacific
- The subthermocline eddy significantly elevated the thermocline mixing through shear instability with $Ri < 1/4$
- The subthermocline eddy acted as dynamic barrier for the downward penetration of wind-generated near-inertial energy

Supporting Information:

- Supporting Information S1

Correspondence to:

W. Zhao,
weizhao@ouc.edu.cn

Citation:

Zhang, Z., Liu, Z., Richards, K., Shang, G., Zhao, W., Tian, J., et al. (2019). Elevated diapycnal mixing by a subthermocline eddy in the western equatorial Pacific. *Geophysical Research Letters*, 46, 2628–2636. <https://doi.org/10.1029/2018GL081512>

Received 30 NOV 2018

Accepted 15 FEB 2019

Accepted article online 19 FEB 2019

Published online 1 MAR 2019

Elevated Diapycnal Mixing by a Subthermocline Eddy in the Western Equatorial Pacific

Zhiwei Zhang¹ , Zhiyu Liu² , Kelvin Richards³, Gong Shang¹, Wei Zhao¹ , Jiwei Tian¹ , Xiaodong Huang¹, and Chun Zhou¹

¹Physical Oceanography Laboratory/IAOS, Ocean University of China, and Qingdao National Laboratory for Marine Science and Technology, Qingdao, China, ²State Key Laboratory of Marine Environmental Science, and Department of Physical Oceanography, College of Ocean and Earth Sciences, Xiamen University, Xiamen, China, ³International Pacific Research Center and Department of Oceanography, University of Hawaii at Manoa, Honolulu, HI, USA

Abstract Diapycnal mixing plays an important role in modulating upper-ocean heat content of the western equatorial Pacific (WEP) that profoundly impacts the global climate. Given the sparsity of long-term in situ observations, the mechanisms driving thermocline mixing in the WEP remain poorly understood. Here, based on yearlong mooring measurements in the WEP, we first report that the occurrence of shear instability was significantly enhanced by an anticyclonic subthermocline eddy (STE). As a result of strong subinertial velocity shear and weakened stratification associated with the STE, the Richardson number was decreased below $1/4$ and the estimated diapycnal diffusivity was increased by 400%. Moreover, contrary to surface-intensified anticyclonic eddies, the STE appeared to act as a dynamic barrier for downward penetration of wind-generated near-inertial energy, which may also fertilize mixing near the upper thermocline. Given the frequent occurrence of STEs, they may play a pivotal role in driving thermocline mixing in the WEP.

Plain Language Summary Turbulent mixing across density surfaces can bring cold water from the deep to the near-surface layer of the ocean; it therefore modulates the upper-ocean heat content of the western equatorial Pacific, which is critically important for the global climate system. Here, based on long-term velocity and temperature measurements from a bottom-anchored mooring, we for the first time found that the strong currents associated with a subsurface ocean eddy strongly elevated the upper-ocean mixing in the western equatorial Pacific through increasing the occurrence of shear instability, which occurs in stratified shear flows when the destabilizing effects of the velocity shear exceeds the stabilizing effects of the density stratification. Given their frequent occurrence in the western equatorial Pacific, the subsurface eddies may provide an important route to driving turbulent mixing therein.

1. Introduction

The western equatorial Pacific (WEP) is a crossroad where water masses of different origins converge and exchange their properties (Fine et al., 1994). Transformation of these different sourced waters strongly modulates thermocline properties and upper-layer heat content of the Pacific warm pool (Grenier et al., 2011; Hu et al., 2015; Meinen & McPhaden, 2000), during which process turbulent mixing across density surfaces (i.e., diapycnal mixing) is believed to play a fundamental role (Koch-Larrouy et al., 2007; Li & Wang, 2012; Lukas et al., 1996). A thorough understanding of the physics driving diapycnal mixing in the WEP is a prerequisite for improving parameterization of mixing processes, which is of vital importance for ocean models to precisely simulate the warm pool and its variability.

Conventionally, diapycnal mixing in the ocean interior is thought to be primarily associated with the breaking of internal gravity waves (e.g., MacKinnon et al., 2017). However, because the energy transfer rate due to internal wave-wave interactions is generally proportional to the local inertial frequency, internal wave breaking, and thus the induced turbulent mixing are strongly suppressed at low latitudes (Gregg et al., 2003; Henyey et al., 1986; Liu et al., 2017). Regardless of this fact, many observational studies in the eastern equatorial Pacific have demonstrated that the large subinertial velocity shears of the South Equatorial Current and the Equatorial Undercurrent (EUC) can also induce strong thermocline mixing, and the mixing intensity can be significantly modulated by Tropical Instability Waves on different time scales (e.g., Liu et al., 2016, 2019; Moum et al., 2012; Smyth & Moum, 2013).

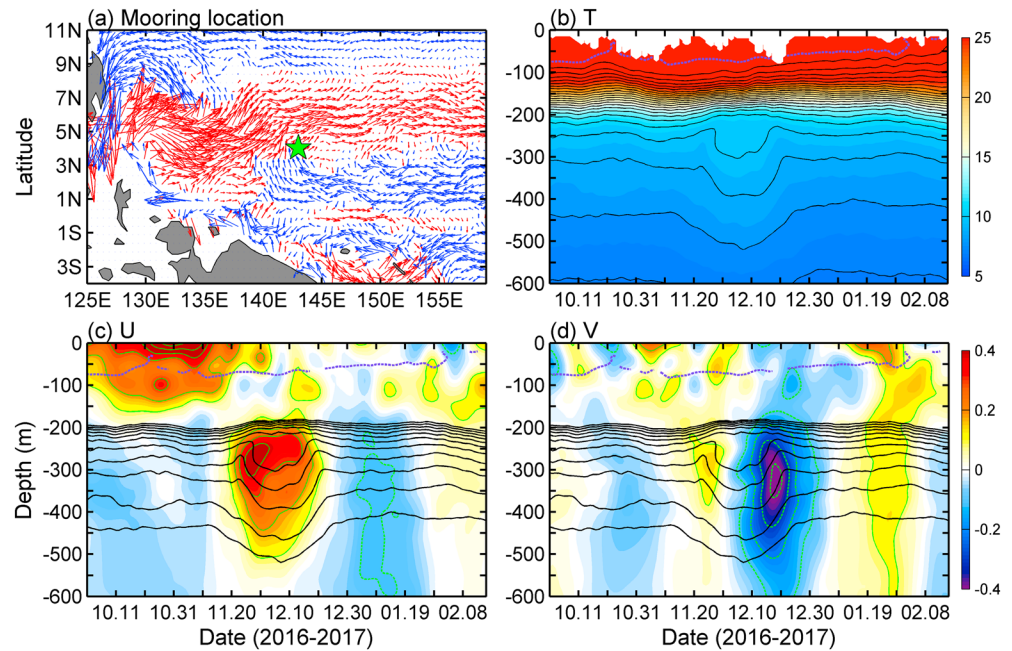


Figure 1. (a) Location of the mooring P3 (green pentagram) that captured the subthermocline eddy. Vectors denote the annual mean altimeter surface geostrophic velocity with the eastward and westward components in red and blue, respectively. (b) Depth-time plot of the temperature (color shading) at P3 with a contour interval of 1 °C (black lines). (c) Depth-time plot of the zonal subinertial velocity (color shading) with a contour interval of 0.1 m/s (green lines). Black lines denote isotherms of every 0.5 °C from 8 to 13 °C. Panel (d) is the same as (c) but for the meridional velocity. Purple dashed line is the 30 °C isotherm that roughly delineates the base of the mixed layer.

Compared with the widely studied eastern equatorial Pacific, thermocline mixing-related observations were, however, relatively rare in the WEP. Recently, by analyzing microstructure data collected at several transects in the WEP, Richards et al. (2012, 2015) have suggested that thermocline mixing in the WEP was dominated by small-vertical-scale velocity structures (SVSs), which appeared to be subject to significant temporal variations. Modeling study points to inertial instability (Natarov & Richards, 2015) as being a prime candidate for the SVSs and associated elevated diapycnal diffusivity, although on one occasion when the shear was weak, double-diffusive processes were found to be important (Lee et al., 2014). Due to the lack of long-term continuous high vertical resolution observations, nevertheless, the relative contributions of these mechanisms to the overall mixing remain unclear. The more recent microstructure measurements in the western boundary of the WEP suggest that thermocline mixing was generally weak with the diapycnal diffusivity $\kappa_p \sim O(10^{-6})$ m²/s, and elevated mixing was only found where geostrophic shear was significant (Liu et al., 2017). In addition, based on long-term ADCP (acoustic Doppler current profiler) measurements from several subsurface moorings, Zhang et al. (2018) pointed out that thermocline mixing in the WEP may be to a large degree associated with the strong subinertial velocity shear between the EUC and Equatorial Intermediate Current. As such, the driving mechanisms of thermocline mixing in the WEP remain elusive.

To this end, we report here on the first observation of enhanced occurrence of shear instability by a subthermocline eddy (STE) in the WEP. The STEs are a special type of oceanic eddies characterized by lens-like thermohaline structures beneath the main thermocline (McWilliams, 1985). Although STEs have been observed in many regions of the world ocean (e.g., Li et al., 2017; Lin et al., 2017; Pelland et al., 2013; Zhang et al., 2015), to our best knowledge, no STE has ever been clearly documented in the WEP with concurrent velocity and hydrographic measurements. Here, based on yearlong ADCP and temperature/salinity chain data collected from a mooring deployed at (143°E, 4°N), we present observations of a warm-core STE with strong velocity below 200 m (Figure 1). Further analysis suggested that the strong velocity shear of STE greatly destabilized the flow by reducing the Richardson number (Ri) below 1/4, which increased the inferred diapycnal diffusivity around the thermocline by a factor of 4. The available data also allow an analysis of the influence of STE on the behaviors of wind-driven near-inertial waves (NIWs).

2. The Data

In order to investigate the characteristics, as well as interactions and energy cascades among the multiscale ocean dynamical processes, the Northwestern Pacific Eddies, Internal waves and Mixing Experiment (NPEIM) was initiated in 2015–2016, during which 17 subsurface moorings were deployed along the 143°E transect between the equator and 22°N (Zhang et al., 2018). The field data analyzed here are from the mooring P3 at ~4°N (Figure 1a) deployed from January 2016 to February 2017. This mooring was equipped with two 75-kHz ADCPs (one looked upward and the other downward) at ~500 m to measure the upper-ocean velocity profile (above 1,000 m) every half an hour. In addition to ADCPs, several CTDs and dozens of temperature loggers were mounted on the upper 1,000 m of the mooring to observe the temperature (and also salinity from CTDs) every 5 min. The ADCPs sampled with a bin size of 16 m, and the vertical resolution of temperature measurements ranged from 10 m at ~30 m to 40 m below ~500 m. The quality-controlled and vertically interpolated hourly data with a uniform 10-m resolution were used for analysis in this study. Detailed mooring configurations and procedures of data processing can be found in Zhang et al. (2018).

To help interpret the mooring observations, the 1/4° daily gridded altimeter sea level anomaly (SLA) and surface geostrophic velocity data (<http://marine.copernicus.eu/>) during the observation period were also used in this study. Additionally, the 1/4° 6-hourly ECMWF interim reanalysis wind data (<http://apps.ecmwf.int/datasets/>), the IPRC monthly Argo product (<http://apdrc.soest.hawaii.edu/>), and the Argo profiles around the mooring location (<http://www.argo.ucsd.edu/>) were also used.

3. Results

3.1. Characteristics of the STE

Figures 1b–1d show the depth-time plots of the temperature, and zonal and meridional velocities observed at P3, respectively. To focus on the subinertial signals, both the temperature and velocities shown here have been 10-day low-pass filtered. From late November to late December 2016, a lens-like structure with nearly homogenous temperature was observed at ~200–300 m (Figure 1b). The core of the lens (at ~250 m), which was roughly bounded by the 10 °C and 11 °C isotherms, was located just beneath the main thermocline (at ~150 m; Figure 2a). During the lens period, the 10 °C isotherm was deepened by 70 m (from 230- to 300-m depth), while the 11 °C isotherm was only slightly raised (from 210 to 200 m). Although the thickness of the nearly well-mixed lens was only 100 m, its dynamical influence in the vertical was much broader. Corresponding to the deepened isotherms associated with the lens, it showed a positive dynamical height anomaly (HA) between 160 and 700 m (Figure S1 in the supporting information). Near the surface, however, the HA displacement associated with the lens was quite small (<1 cm) and therefore can hardly be detected by satellite altimeter given its limited measuring accuracy.

Accompanying the lens-like thermal structure, there existed strong subinertial currents below the thermocline (Figures 1c–1d). The maximum absolute velocity reached 0.48 m/s at 270 m, which was 6 times of the annual mean absolute velocity at this depth (which was 0.08 m/s, excluding the lens period between 20 November and 20 December). Above the lens-core depth, the subinertial currents were sharply weakened with decreasing depth, in agreement with the vertical distribution of stratification and HA. For the meridional velocity, the large positive and negative values occurred at the front and rear peripheries of the lens-like thermal structure, respectively. If assuming that the lens generally propagated westward due to the planetary β effect (e.g., Collins et al., 2013), this mooring-observed meridional velocity variation would indicate an anticyclonic circulation pattern surrounding the lens. These thermal and velocity characteristics demonstrated that the lens-like structure corresponded to a STE. In contrast to the meridional velocity, the zonal velocity remained positive throughout the “STE” period. This may suggest that it was the northern part of the anticyclonic STE that had been documented by the mooring.

In addition to the mooring P3, the same STE was also synchronously captured by the mooring P2 (143°E, 2°N). Compared to the observed features at P3, the STE at P2 showed smaller lens thickness and westward dominant velocity (not shown). This suggests that it was the southern margin of the STE that crossed the P2 and therefore indicates that the STE’ radius was around 110 km (i.e., half the distance between P2 and P3). Assuming that the STE was in solid body rotation, and that mooring P3 had observed the maximum swirl

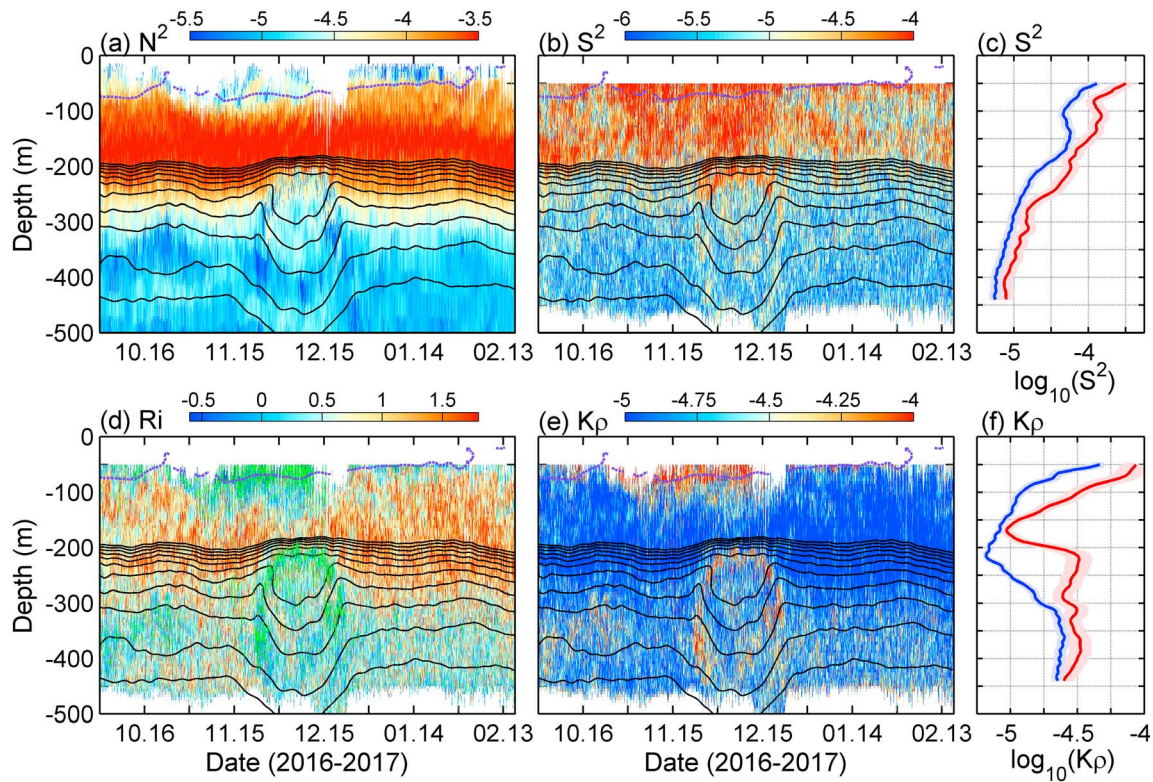


Figure 2. (a, b, d, e) Depth-time plots of N^2 , S^2 , Ri , and K_ρ at P3, respectively. Black and purple lines indicate the isotherms same as in Figure 1c. The Ri values lower than 1/4 in (d) are marked with green dots. Note that all the colorbars are in logarithmic scale (\log_{10}). (c) Mean S^2 profile within (red) and outside of (blue) the subthermocline eddy. Shadings denote the corresponding 95% confidence interval computed using the bootstrap method. Panel (f) is the same as (c) but for K_ρ .

velocity of the STE (U_s , 0.48 m/s at ~ 270 m), we can give a lower-bound estimate of the STE's vorticity using $\zeta \approx -U_s/110$ km. This estimation results in a ζ of $-4.4 \times 10^{-6} \text{ s}^{-1}$, which was 57% of the planetary vorticity at 3°N (the presumed latitude of STE center). Given the fact that the STE has a radius smaller than the first baroclinic deformation radius (~ 250 km according to Chelton et al., 1998) and that its ζ is nonnegligible compared to planetary vorticity, the STE documented here should be in the category of submesoscale coherent vortices (McWilliams, 1985; Zhang et al., 2015).

3.2. Elevated Diapycnal Mixing by the STE

In Figures 2a and 2b we show the hourly squared buoyancy frequency ($N^2 = -g/\rho_0 \cdot \partial\rho/\partial z$) and velocity shear variance ($S^2 = |\partial u/\partial z|^2 + |\partial v/\partial z|^2$) at P3, respectively. In these formulas, g is the acceleration due to gravity, ρ the density, $\rho_0 = 1,030 \text{ kg/m}^3$ is a reference density, and u and v denote the zonal and meridional velocities, respectively. Because salinity measurements on the mooring were too coarse, the IPRC monthly Argo salinity data were used here in the density computations (Zhang et al., 2018). Corresponding to the lens-like isotherm distributions, the stratification within and surrounding the STE was greatly reduced (Figure 2a). At the depth of 200–300 m, the time-mean N^2 during the “STE” period (20 November to 20 December) was only 45–70% of that during the “no-STE” period (1 October to 10 February excluding the “STE” period; supporting information Figure S2a). Because of the convex isotherms near the upper boundary of the STE, N^2 was enhanced between 120 and 180 m (increased by 30% at 150 m). Besides the notable variation of N^2 , the observed S^2 was also prominently enhanced during the “STE” period, especially around the upper and lateral peripheries of the STE (Figure 2b). The ratio of the time-mean S^2 between the “STE” and “no-STE” periods shows two peaks, being 3.2 and 2.8, and located at 110 m and 220 m, respectively (Figures 2c and S2b).

Corresponding to the strong velocity shear mentioned above, the Richardson number ($Ri = N^2/S^2$), a metric of shear instability, was greatly reduced during the STE period (Figure 2d). At the depths of the STE, a large

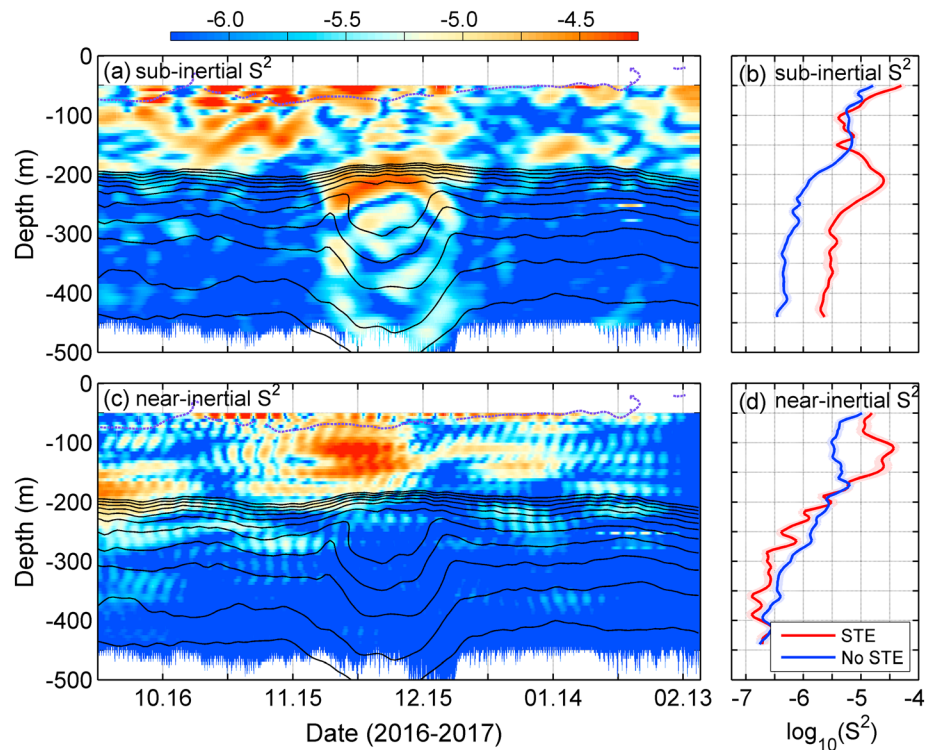


Figure 3. Panels (a, b) and (c, d) are the same as Figures 2b and 2c but for the subinertial and near-inertial S^2 , respectively.

portion of Ri values became below $1/4$, suggesting that strong shear instabilities and therefore enhanced turbulent mixing may have occurred there (e.g., Thorpe, 2005). In contrast, Ri remained relatively high near the upper thermocline (at 100–200 m) due to the strong stratification, although S^2 was also enhanced there. To further evaluate the diapycnal mixing associated with the STE, we estimated the diapycnal diffusivity (K_p) from the Ri -based parameterization devised by Liu et al. (2017): $K_p = K_0 + K_m(1 + Ri/0.25)^{-1}$, where $K_0 = 2.1 \times 10^{-6} \text{ m}^2/\text{s}$ represents the background mixing presumably sustained by breaking of internal waves, and $K_m = 1.9 \times 10^{-4} \text{ m}^2/\text{s}$ is the maximum diffusivity corresponding to vanishing Ri . This parameterization was developed in a similar spirit of Pacanowski and Philander (1981), and the constants K_0 and K_m were determined by least squares regression based on dozens of microstructure profiles in the WEP. Similar to S^2 and the inverse Ri , the diapycnal diffusivity K_p was significantly elevated during the STE period (Figures 2e and 2f), especially near the surface and around the periphery of the STE. Below the near-surface layer, the largest STE-period-mean K_p occurred at 220 m, just around the STE's upper periphery beneath the thermocline. This elevated K_p reached $3.3 \times 10^{-5} \text{ m}^2/\text{s}$, nearly 4 times larger than that outside of the STE (Figure 2f).

To explore the mechanism of the increased S^2 during the STE period, we further decomposed the velocity shear into the subinertial, near-inertial, diurnal, and semidiurnal components, respectively, which are thought as four main contributors of the finescale velocity shear in the ocean interior (MacKinnon et al., 2017). Because the subinertial and near-inertial S^2 were much larger than that at diurnal and semidiurnal frequencies during the STE period, only the former two components were analyzed in detail (Figure 3). The cross term of subinertial and near-inertial shears was found to be substantially smaller during the STE period and is therefore omitted in our further analysis. The subinertial (near-inertial) velocity used to calculate the corresponding shear was obtained through a fourth-order Butterworth low-pass (band-pass) filter with a cutoff frequency of $0.75f$ ($0.75f$ – $1.25f$), where f is the local inertial frequency. Corresponding to the strong subinertial velocity of the STE, the subinertial S^2 below 180 m (to over 450 m) was greatly enhanced during the STE period, with the time-mean magnitudes being 4–20 times of the background value (Figure 3b). The maximum increase of subinertial S^2 (twentyfold) occurred at 220 m, coinciding with the depth of the subthermocline K_p (and Ri^{-1}) peak. Above the 180 m, however, the subinertial S^2 was not

significantly different from the background value. With regard to the near-inertial S^2 , it displayed an overall opposite vertical distribution with the subinertial S^2 during the STE period. Specifically, the near-inertial S^2 was increased by a factor of 2–10 above the STE's upper periphery but decreased by 30–70% below that. The maximum increase was located around 110 m, in agreement with the first peak of the S^2 ratio between the STE and no-STE periods (supporting information Figure S2b).

To summarize, it is evident from Figures 2 and 3 that the STE significantly elevated thermocline mixing in the WEP through shear instability of the eddy-induced currents. The Richardson number Ri was greatly reduced (to below 1/4) as a combination of enhanced subinertial S^2 and weakened N^2 . During the STE period, the near-surface-layer S^2 was also increased due to the coincident energetic NIWs possibly forced by strong winds at that time (supporting information Figure S3; Dohan & Davis, 2011). However, the strong near-inertial shears could not penetrate downward into the STE and they seemed to moderately elevate the mixing at the upper thermocline (Figures 2e and 2f).

3.3. Impact of the STE on Near-Inertial Waves

Previous studies have suggested that surface-intensified anticyclonic eddies (AEs) with negative vorticity (ζ) can trap wind-generated NIWs and promote their downward propagations by reducing the effective inertial frequency, that is, $f_{\text{eff}} = f + \zeta/2$ (Kunze, 1985; Lee & Niiler, 1998; Zhang et al., 2018). Contrary to surface-intensified AEs, nevertheless, the anticyclonic STE documented here does not appear to have facilitated downward propagation of the wind-driven NIWs. In fact, during the STE period, both the near-inertial energy and S^2 were found to be prominently weakened below 200 m. Instead, those in 100–150 m were strengthened in this period (Figures 3c, 3d, and S3b). Here we offer two possible explanations for this seemingly peculiar phenomenon.

First of all, the strong subinertial velocity shear of the STE may have caused reflections of the downward propagating NIWs (Byun et al., 2010). To elaborate this point, we decomposed the near-inertial velocity into clockwise and counterclockwise rotating components (whose energy propagates downward and upward, respectively) using the rotary decomposition (MacKinnon et al., 2013). Indeed, we found that following the strong wind-forced downward propagating NIWs, an episode with enhanced upward going energy occurred during and shortly after the STE event (Figures 4c and 4d). According to the linear internal wave theory (see the dispersion relation in equation (1)), the vertical group velocity Cg_z of a NIW (equation (2)) can reverse its direction when the nondimensional parameter $\mu \equiv \frac{f|k_x||k_z|}{N^2 k_H^2} \left(\left| \frac{\partial U}{\partial z} \right| + \left| \frac{\partial V}{\partial z} \right| \right)$ exceeds unity (Byun et al., 2010).

$$\omega - f_{\text{eff}} \approx \frac{N^2}{2f} \cdot \frac{k_H^2}{k_z^2} + \frac{1}{k_z} \left(\frac{\partial U}{\partial z} k_y - \frac{\partial V}{\partial z} k_x \right) \quad (1)$$

$$Cg_z = \frac{\partial \omega}{\partial k_z} \approx -\frac{N^2 k_H^2}{f \cdot k_z^3} - \frac{1}{k_z^2} \left(\frac{\partial U}{\partial z} k_y - \frac{\partial V}{\partial z} k_x \right) \quad (2)$$

where ω is the wave frequency, U (V) is background zonal (meridional) velocity, k_x , k_y , and k_z are the zonal, meridional, and vertical wave numbers, respectively, and $k_H = \sqrt{k_x^2 + k_y^2}$. Using the $\left| \frac{\partial U}{\partial z} \right| + \left| \frac{\partial V}{\partial z} \right|$ ($4.5 - 8.5 \times 10^{-3} \text{ s}^{-1}$) and the typical stratification ($N = 5 \times 10^{-3} \text{ s}^{-1}$) and NIW k_z ($k_z = 2\pi/80 \text{ m}^{-1}$, estimated based on the cross-zero points of horizontal velocity in vertical) observed near the upper periphery of the STE (around 200 m), and assuming that the NIW has a horizontal wavelength of 200 km (Simmons & Alford, 2012; this should be an upper-bound value because the mooring P4 at 6°N did not capture the same NIWs), we obtain $\mu \approx 2.3 - 4.3$, which suggests the possibility of NIW upward reflection by the STE. The reflection of NIWs made the near-inertial energy converge at the upper thermocline above the STE, which may have increased near-inertial S^2 and then elevated diapycnal diffusivity therein.

Second, according to the dispersion relation of NIWs (equation (1)), the variations of f_{eff} and N^2 can significantly modulate k_z of NIWs and hence the near-inertial S^2 (Kunze, 1985). As the unreflected NIWs continuously propagated downward, they would feel decreased f_{eff} ($\zeta < 0$) and weakened N^2 within the STE, due to which the NIW k_z and S^2 were greatly reduced. And vice versa, the strong stratification above the STE tended

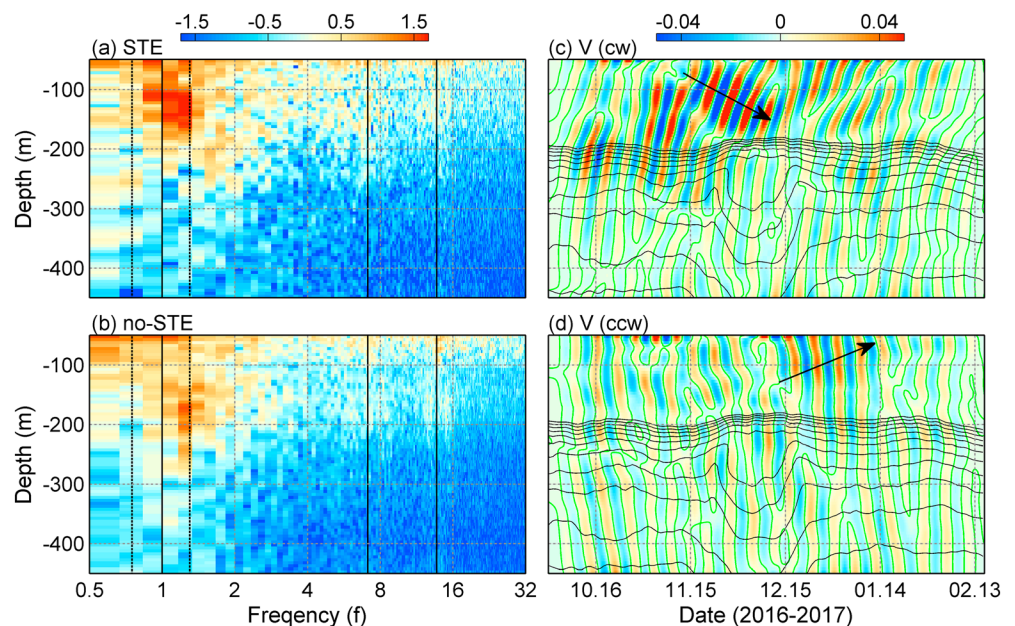


Figure 4. Power spectrum density of velocity shear (in \log_{10}) plotted as a function of depth during (a) STE period and (b) no-STE period. The frequency is normalized by the local inertial frequency at P3. The three vertical solid lines from left to right denote the inertial, diurnal, and semidiurnal frequencies, respectively. The $0.75f$ and $1.25f$ are indicated by vertical dashed lines. (c, d) Depth-time plots of the clockwise and counter-clockwise rotating component of the near-inertial meridional velocity, respectively. Black lines are same as Figure 3a. Black arrows indicate the vertical propagation of near-inertial wave energy. STE = subthermocline eddy.

to increase the NIW k_z , which can partially explain the large near-inertial S^2 therein in addition to the NIW reflection. Note also that the enhanced N^2 due to the elevated isopycnals above the STE may have also played an important role in the above-described process (supporting information Figure S2a). Additionally, because the estimated phase velocity ($C_p = \omega/k_H \approx 0.32$ m/s) was smaller than U_s of the STE, it may undergo critical layer processes (where C_p equals the eddy velocity) near the upper periphery of STE, which may be another reason accounting for the enhanced NIW k_z (Munk, 1981).

4. Summary and Discussion

Based on in situ velocity and temperature data collected from a mooring at (143°E , 4°N), we have for the first time reported that the occurrence of shear instability was enhanced by an anticyclonic STE in the WEP due to eddy-induced strong subinertial currents. Moreover, we have shown that, although the STE had negative ζ , it did not act as an “inertial chimney” for NIWs like surface-intensified AEs because of its greatly weakened vorticity toward the surface (e.g., Kunze, 1985; Zhang et al., 2018). Instead, near-inertial energy and S^2 were greatly reduced within the STE presumably due to NIW reflection and wavelength stretching. As the STE had hindered downward propagation of wind-driven NIWs, near-inertial energy converged near the upper thermocline, which might have further energized turbulent mixing therein. We acknowledge that the diapycnal diffusivity K_p analyzed in this study was estimated from velocity and hydrographic measurements using an empirical parameterization rather than directly from in situ microstructure data. This, nevertheless, should not affect our main conclusion, since it is qualitative property of K_p (i.e., elevation by the STE) rather than its precise value that is emphasized here.

By examining all synchronous Argo profiles in the vicinity of the moorings, we found that four successive profiles from Float 2901548 (at $144.5\text{--}145.1^\circ\text{E}$, $2.0\text{--}2.4^\circ\text{N}$) happened to capture a similar STE on 12 November to 22 December 2016 (supporting information Figures S4a and S4b). Given their close occurrence in time and geographic location, and similar temperature profiles, we can conclude that the mooring and Argo data documented the same STE. Following the approach of Zhang et al. (2015), we can roughly trace the origin of the STE based on its core density and salinity and found that the STE probably originated from

the coastal region of New Guinea (supporting information Figure S4c). Considering that the STE's origin region is impacted by the New Guinea Coastal Undercurrent (NGCU) and its vertical level is close to the core of NGCU (Cravatte et al., 2011; Davis et al., 2012), generation mechanism of this STE may be associated with NGUC topography interaction in a similar manner to that proposed for the California Undercurrent Eddies (Molemaker et al., 2015).

Based on the estimated K_ρ and the Osborn relation ($K_\rho = 0.2 \frac{\epsilon}{N^2}$), we can roughly estimate that the STE had a mean dissipation rate (ϵ) of $2.7 \times 10^{-9} \text{ m}^2/\text{s}^3$ (averaged over 200–500 m) during the eddy period. Dividing the sum of kinetic and available potential energy of the STE (the mean value was estimated to be $7.6 \times 10^{-2} \text{ m}^2/\text{s}^2$) by the estimated ϵ gives rise to a time scale of ~320 days, which agrees with the previously reported lifespan of STE in the order of magnitude (McWilliams, 1985). This suggests that the self-induced subinertial shear instability reported in this study may provide an important route for the dissipation of STE when the external forcings are generally weak beneath the thermocline.

Previous observational and modeling studies have suggested that STEs may be a common phenomenon that frequently occurs in the WEP (Chiang & Qu, 2013; Chiang et al., 2015; Wang et al., 2015; Zhang et al., 2014). Given that the STEs can effectively enhance turbulent mixing and that breaking of internal waves at low latitudes is suppressed, the frequently occurring STEs may provide an important route to energizing thermocline mixing in the WEP. The role of STE-induced mixing in the WEP upper-layer heat budget needs to be evaluated in future with more specifically designed observations.

Acknowledgments

The authors thank the valuable comments from three anonymous reviewers that help improve the paper. Z. Z., W. Z., and J. T. were supported by the National Key R&D Program of China (2016YFC1402605), the National Natural Science Foundation of China (NSFC; 41706005, 91628302, and 41521091), and the National Program on Global Change and Air-Sea Interaction (GASI-02-PAC-ST-MSwin, GASI-02-PAC-ST-MSaut, GASI-IPOVAI-01-03, and GASI-IPOVAI-01-02). Z. L.'s participation of this work was supported by the NSFC (41622601 and 91858201) and the National Key R&D Program of China (2016YFC1401404). The moored data analyzed in this study can be obtained at this website (<https://jumpshare.com/v/BjbeZsrI9KJYIB066yU>).

References

- Byun, S., Park, J. J., Chang, K., & Schmitt, R. W. (2010). Observation of near-inertial wave reflections within the thermostad layer of an anticyclonic mesoscale eddy. *Geophysical Research Letters*, *37*, L01606. <https://doi.org/10.1029/2009GL041601>
- Chelton, D. B., Deszoeke, R. A., Schlax, M. G., El Naggar, K., & Siwertz, N. (1998). Geographical variability of the first baroclinic Rossby radius of deformation. *Journal of Physical Oceanography*, *28*(3), 433–460. [https://doi.org/10.1175/1520-0485\(1998\)028<0433:GVOTFB>2.0.CO;2](https://doi.org/10.1175/1520-0485(1998)028<0433:GVOTFB>2.0.CO;2)
- Chiang, T., Wu, C., Qu, T., & Hsin, Y. (2015). Activities of 50–80 day subthermocline eddies near the Philippine coast. *Journal of Geophysical Research: Oceans*, *120*, 3606–3623. <https://doi.org/10.1002/2013JC009626>
- Chiang, T. L., & Qu, T. (2013). Subthermocline eddies in the western equatorial Pacific as shown by an eddy-resolving OGCM. *Journal of Physical Oceanography*, *43*(7), 1241–1253. <https://doi.org/10.1175/JPO-D-12-0187.1>
- Collins, C. A., Margolina, T., Rago, T. A., & Ivanov, L. (2013). Looping RAFOS floats in the California current system. *Deep Sea Research Part II: Topical Studies in Oceanography*, *85*(85), 42–61. <https://doi.org/10.1016/j.dsr2.2012.07.027>
- Cravatte, S., Ganachaud, A., Duong, Q. P., Kessler, W. S., Eldin, G., & Dutrieux, P. (2011). Observed circulation in the Solomon Sea from SADCP data. *Progress in Oceanography*, *88*(1-4), 116–130. <https://doi.org/10.1016/j.pocean.2010.12.015>
- Davis, R. E., Kessler, W. S., & Sherman, J. T. (2012). Gliders measure western boundary current transport from the South Pacific to the equator. *Journal of Physical Oceanography*, *42*(11), 2001–2013. <https://doi.org/10.1175/JPO-D-12-022.1>
- Dohan, K., & Davis, R. E. (2011). Mixing in the transition layer during two storm events. *Journal of Physical Oceanography*, *41*(1), 42–66. <https://doi.org/10.1175/2010JPO4253.1>
- Fine, R. A., Lukas, R., Bingham, F. M., Warner, M. J., & Gammon, R. H. (1994). The western equatorial Pacific: A water mass crossroads. *Journal of Geophysical Research*, *99*(C12), 25,063–25,080. <https://doi.org/10.1029/94JC02277>
- Gregg, M. C., Sanford, T. B., & Winkel, D. P. (2003). Reduced mixing from the breaking of internal waves in equatorial waters. *Nature*, *422*(6931), 513–515. <https://doi.org/10.1038/nature01507>
- Grenier, M., Cravatte, S., Blanke, B., Menkes, C., Koch-Larrouy, A., Durand, F., et al. (2011). From the western boundary currents to the Pacific equatorial undercurrent: Modeled pathways and water mass evolutions. *Journal of Geophysical Research*, *116*, C12044. <https://doi.org/10.1029/2011JC007477>
- Heney, F. S., Wright, J., & Flatte, S. M. (1986). Energy and action flow through the internal wave field: An eikonal approach. *Journal of Geophysical Research*, *91*(C7), 8487–8495. <https://doi.org/10.1029/JC091C07p08487>
- Hu, D., Wu, L., Cai, W., Gupta, A. S., Ganachaud, A., Qiu, B., et al. (2015). Pacific western boundary currents and their roles in climate. *Nature*, *522*(7556), 299–308. <https://doi.org/10.1038/nature14504>
- Koch-Larrouy, A., Madec, G., Bouruet-Aubertot, P., Gerkema, T., Bessières, L., & Molcard, R. (2007). On the transformation of Pacific water into Indonesian throughflow water by internal tidal mixing. *Geophysical Research Letters*, *34*, L04604. <https://doi.org/10.1029/2006GL028405>
- Kunze, E. (1985). Near-inertial wave propagation in geostrophic shear. *Journal of Physical Oceanography*, *15*(5), 544–565. [https://doi.org/10.1175/1520-0485\(1985\)015<0544:NIWPIG>2.0.CO;2](https://doi.org/10.1175/1520-0485(1985)015<0544:NIWPIG>2.0.CO;2)
- Lee, C., Chang, K.-I., Lee, J. H., & Richards, K. J. (2014). Vertical mixing due to double diffusion in the tropical western Pacific. *Geophysical Research Letters*, *41*, 7964–7970. <https://doi.org/10.1002/2014GL061698>
- Lee, D. K., & Niiler, P. P. (1998). The inertial chimney: The near-inertial energy drainage from the ocean surface to the deep layer. *Journal of Geophysical Research*, *103*(C4), 7579–7591. <https://doi.org/10.1029/97JC03200>
- Li, C., Zhang, Z., Zhao, W., & Tian, J. (2017). A statistical study on the subthermocline submesoscale eddies in the northwestern Pacific Ocean based on Argo data. *Journal of Geophysical Research: Oceans*, *122*, 3586–3598. <https://doi.org/10.1002/2016JC012561>
- Li, Y., & Wang, F. (2012). Spreading and salinity change of North Pacific tropical water in the Philippine Sea. *Journal of Oceanography*, *68*(3), 439–452. <https://doi.org/10.1007/s10872-012-0110-3>
- Lin, H., Hu, J., Liu, Z., Belkin, I. M., Sun, Z., & Zhu, J. (2017). A peculiar lens-shaped structure observed in the South China Sea. *Scientific Reports*, *7*(1), 478. <https://doi.org/10.1038/s41598-017-00593-y>

- Liu, C., Köhl, A., Liu, Z., Fan, W., & Stammer, D. (2016). Deep-reaching thermocline mixing in the equatorial Pacific cold tongue. *Nature Communications*, 7(1), 11576. <https://doi.org/10.1038/ncomms11576>
- Liu, C., Wang, X., Köhl, A., Wang, F., & Liu, Z. (2019). The northeast-southwest oscillating equatorial mode of the tropical instability wave and its impact on equatorial mixing. *Geophysical Research Letters*, 46, 218–225. <https://doi.org/10.1029/2018GL080226>
- Liu, Z., Lian, Q., Zhang, F., Wang, L., Li, M., Bai, X., et al. (2017). Weak thermocline mixing in the North Pacific low-latitude western boundary current system. *Geophysical Research Letters*, 44, 10,530–10,539. <https://doi.org/10.1002/2017GL075210>
- Lukas, R., Yamagata, T., & McCreary, J. P. (1996). Pacific low-latitude western boundary currents and the Indonesian throughflow. *Journal of Geophysical Research*, 101(C5), 12,209–12,216. <https://doi.org/10.1029/96JC01204>
- MacKinnon, J. A., Alford, M. H., Sun, O., Pinkel, R., Zhao, Z., & Klymak, J. (2013). Parametric subharmonic instability of the internal tide at 29°N. *Journal of Physical Oceanography*, 43(1), 17–28. <https://doi.org/10.1175/JPO-D-11-0108.1>
- MacKinnon, J. A., Zhao, Z., Whalen, C. B., Waterhouse, A. F., Trossman, D. S., Sun, O. M., et al. (2017). Climate process team on internal-wave driven ocean mixing. *Bulletin of the American Meteorological Society*, 98(11), 2429–2454. <https://doi.org/10.1175/BAMS-D-16-0030.1>
- McWilliams, J. C. (1985). Submesoscale, coherent vortices in the ocean. *Reviews of Geophysics*, 23(2), 165–182. <https://doi.org/10.1029/RG023i002p00165>
- Meinen, C. S., & McPhaden, M. J. (2000). Observations of warm water volume changes in the equatorial Pacific and their relationship to El Niño and La Niña. *Journal of Climate*, 15(20), 3551–3559.
- Molemaker, M. J., McWilliams, J. C., & Dewar, W. K. (2015). Submesoscale instability and generation of mesoscale anticyclones near a separation of the California undercurrent. *Journal of Physical Oceanography*, 45(3), 613–629. <https://doi.org/10.1175/JPO-D-13-0225.1>
- Moum, J. N., Lien, R. C., Perlin, A., Nash, J. D., Gregg, M. C., & Wiles, P. J. (2012). Sea surface cooling at the equator by subsurface mixing in tropical instability waves. *Nature Geoscience*, 2(11), 761–765.
- Munk, W. (1981). Internal waves and small-scale processes. In B. A. Warren & C. Wunsch (Eds.), *Evolution of physical oceanography* (pp. 264–291). Cambridge: MIT Press.
- Natarov, A., & Richards, K. J. (2015). Persistent presence of small vertical scale velocity features during three-dimensional equilibration of equatorial inertial instability. *Physics of Fluids*, 27(8), 84109. <https://doi.org/10.1063/1.4928319>
- Pacanowski, R. C., & Philander, S. G. H. (1981). Parameterization of vertical mixing in numerical models of tropical oceans. *Journal of Physical Oceanography*, 11(11), 1443–1451. [https://doi.org/10.1175/1520-0485\(1981\)011<1443:POVMIN>2.0.CO;2](https://doi.org/10.1175/1520-0485(1981)011<1443:POVMIN>2.0.CO;2)
- Pelland, N. A., Eriksen, C. C., & Lee, C. M. (2013). Subthermocline eddies over the Washington continental slope as observed by Seagliders, 2003–09. *Journal of Physical Oceanography*, 43(10), 2025–2053. <https://doi.org/10.1175/JPO-D-12-086.1>
- Richards, K. J., Kashino, Y., Natarov, A., & Firing, E. (2012). Mixing in the western equatorial Pacific and its modulation by ENSO. *Geophysical Research Letters*, 39, L02604. <https://doi.org/10.1029/2011GL050439>
- Richards, K. J., Natarov, A., Firing, E., Kashino, Y., Soares, S. M., Ishizu, M., et al. (2015). Shear-generated turbulence in the equatorial Pacific produced by small vertical scale flow features. *Journal of Geophysical Research: Oceans*, 120, 3777–3791. <https://doi.org/10.1002/2014JC010673>
- Simmons, H. L., & Alford, M. H. (2012). Simulating the long-range swell of internal waves generated by ocean storms. *Oceanography*, 25(2), 30–41. <https://doi.org/10.5670/oceanog.2012.39>
- Smyth, W. D., & Moum, J. N. (2013). Marginal instability and deep cycle turbulence in the eastern marginal instability and deep cycle turbulence in the equatorial Pacific Ocean. *Geophysical Research Letters*, 40, 6181–6185. <https://doi.org/10.1002/2013GL058403>
- Thorpe, S. A. (2005). *The turbulent ocean* (p. 485). Cambridge: Cambridge University Press. <https://doi.org/10.1017/CBO9780511819933>
- Wang, Q., Zhai, F., Wang, F., & Hu, D. (2015). Intraseasonal variability of the subthermocline current east of Mindanao. *Journal of Geophysical Research: Oceans*, 119, 8552–8566. <https://doi.org/10.1002/2014JC010343>
- Zhang, L., Hu, D., & Hu, S. (2014). Mindanao current/undercurrent measured by a subsurface mooring. *Journal of Geophysical Research: Oceans*, 119, 3617–3628. <https://doi.org/10.1002/2013JC009693>
- Zhang, Z., Li, P., Xu, L., Li, C., Zhao, W., Tian, J., & Qu, T. (2015). Subthermocline eddies observed by rapid-sampling Argo floats in the subtropical northwestern Pacific Ocean in spring 2014. *Geophysical Research Letters*, 42, 6438–6445. <https://doi.org/10.1002/2015GL064601>
- Zhang, Z., Qiu, B., Tian, J., Zhao, W., & Huang, X. (2018). Latitude-dependent finescale turbulent shear generations in the Pacific tropical-extratropical upper ocean. *Nature Communications*, 9(1), 4086. <https://doi.org/10.1038/s41467-018-06260-8>